Experimental support for a simplified approach to CTRW transport models and exploration of parameter interpretation

Scott K. Hansen[1]

[1]Zuckerberg Institute for Water Research, Ben-Gurion University of the Negev

Key Points:

- We show how a simplified, physically-constrained CTRW approach and velocity-independent transition PDFs explain experimental data.
- BTCs at multiple flow rates are fit with true velocities and shared CTRW parameters (with unit time constant) for two physical setups.
- We show by example how distinct sets of CTRW parameters may fit the same BTC ensemble; parameters cannot be interpreted individually.

Corresponding author: Scott K. Hansen, skh@bgu.ac.il

Abstract

We empirically test our earlier theoretical arguments about simplification of continuous-time random walk (CTRW) solute transport models, namely that without loss of generality the velocity-like term, v_ψ, may be set to mean groundwater velocity, the dispersion-like term, D_ψ, defined by a classical, velocity-independent dispersivity, and the so-called time constant, τ, to unity. We also argue that for small-scale heterogeneous advection (HA) and mobile-immobile mass transfer (MIMT) CTRW transition time distributions, $\psi(t)$, are unaffected by mean flow velocity. To experimentally test these claims, we re-analyze two bench-scale transport experiments—one for HA, one for MIMT—each performed at multiple flow rates in otherwise identical conditions, and show it is possible to simultaneously explain all breakthrough curves in each, subject to the above constraints. We compare our calibrations with earlier efforts for the same data sets. In the HA calibration we identify a $\psi(t)$ of the same functional form as previous authors, and which yielded breakthrough predictions essentially identical to theirs, but with greatly differing parameters. This illustrates how values of individual CTRW parameters may not map one-to-one onto underlying physics. We recommend reporting complete model descriptions, discuss how the simplified approach assists in this and other theoretical considerations.

1 Introduction

In a recent paper (Hansen, 2020), we proposed an interpretation of some of the terms of the continuous-time random walk (CTRW) generalized master equation (GME), which allow its 1D form to be written in the following simplified way:

$$\frac{\partial c(x,t)}{\partial t} = \int_0^t M(t-t') \left(-\bar{v} \frac{\partial c(x,t')}{\partial x} + \alpha \bar{v} \frac{\partial^2 c(x,t')}{\partial x^2} \right) dt'. \tag{1}$$

Here, c [ML^{-3}] is concentration, $M(t)$ [T^{-1}] is a temporal memory function, $\bar{v}$ [LT^{-1}] is mean groundwater velocity, and α [L] is a standard Fickian dispersivity, generated by multiplication of $\bar{v}$ by some fixed, medium-specific dispersivity, α [L]; x [L] is spatial coordinate, and t [T] is time. On this approach, $M(t)$ is defined in the Laplace domain according the formula:

$$\tilde{M}(s) \equiv \frac{s\tilde{\psi}(s)}{1-\tilde{\psi}(s)}, \tag{2}$$

where superscript tilde denotes the Laplace transform, s [T^{-1}] is the Laplace variable, and $\psi(t)$ [T^{-1}] is the probability distribution function for a subordination mapping representing

the total time taken for solute to complete a transition that would have taken unit time under purely advective-dispersive physics as described by $\bar{v}$ and α.

This approach simplifies and physically constrains the CTRW GME in a number of ways and also provides an interpretation to its parameters. By contrast, in typical usage: (a) the $\bar{v}$ and $\alpha\bar{v}$ are replaced with arbitrary fitting parameters v_ψ and D_ψ that do not generally have any specific relation to groundwater velocity, (b) the definition of M typically contains an arbitrary "time constant" fitting parameter with no specific interpretation, τ [T], in its numerator, and (c) the transition time distribution, $\psi(t)$ has no particular definition; it is an additional fitting "parameter". For clarity, the standard CTRW GME and transformed memory function corresponding to (1-2) are

$$\frac{\partial c(x,t)}{\partial t} = \int_0^t M(t-t') \left(v_\psi \frac{\partial c(x,t')}{\partial x} + D_\psi \frac{\partial^2 c(x,t')}{\partial x^2} \right) dt', \tag{3}$$

$$\tilde{M}(s) \equiv \frac{s\tau\tilde{\psi}(s)}{1-\tilde{\psi}(s)}. \tag{4}$$

Implicitly τ is set to unity in the simplified approach, so the units remain consistent. The simplified approach is based on two ideas which are outlined in more detail in Hansen (2020):

1. It is possible to select the time constant τ so that v_ψ and D_ψ are equal to their Fickian counterparts.
2. The memory function (4) is invariant under the simultaneous transformations $\tau \to 1$, $\tilde{\psi}(s) \to [\tilde{\psi}(s)]^{1/\tau}$.

Two key subsurface transport processes that need to be captured by $\psi(t)$ are (the non-Fickian portion of) local-scale heterogeneous advection (HA), and mobile-immobile mass transfer (MIMT). Elsewhere (Hansen and Berkowitz, 2020b,0), in describing the CTRW-on-a-streamline approach, have argued that both advective heterogeneity and MIMT (including behavior described by multi-rate mass transfer, first-order non-equilibrium mass transfer, and retardation) can be adequately captured by a subordination approach.

We do not believe it has been remarked upon, but a joint implication of the subordination mapping interpretation of $\psi(t)$ alongside the CTRW-on-a-streamline arguments is that $\psi(t)$ should be invariant to mean groundwater velocity under many scenarios. For MIMT, so long as immobilization probability is related to time-in-system rather than distance traveled and the immobilization time pdf is determined by conditions in the immobile

domain alone, it follows that the distribution of delay times due to the MIMT physics is independent of the mean flow velocity in the mobile domain. For HA, it follows from linearity of the groundwater flow equation that velocity fluctuations will scale with fluctuations in the local mean groundwater velocity. We may arbitrarily define a transition to have occurred when solute has traveled $d(\bar{v})$ [L] units along its streamline, where $d(\bar{v})$ is selected as the distance that advection covers in unit time at mean velocity. Because all the velocities scale with $\bar{v}$, $\psi(t)$, defined as the probability distribution for the actual time taken to complete a transition of length d, is unchanged with changes in $\bar{v}$.

The argument above generates testable predictions. If tracer experiments are to be performed across a tank or column under multiple flow rates but otherwise identical conditions, we would expect all the breakthrough curves obtained at the various flow rates to be explained by a single $\psi(t)$, α, and the actual $\bar{v}$ values from the various experiments. Consequently, in this paper we re-analyze results from two experiments that were conducted repeatedly at multiple flow rates: one featuring HA in sand, and one featuring MIMT in the form of matrix diffusion.

For HA, few existing bench-scale data sets were available. A few experiments considered breakthrough at multiple distances in the same apparatus (Silliman and Simpson, 1987; Huang *et al.*, 1995). However, to our knowledge, Levy and Berkowitz (2003) present the only data on breakthrough curves obtained at multiple flow rates in the same statistically stationary, heterogeneous flow cell. We used this experimental data set for our analyses. For MIMT, a greater variety of published data was available. Both van Genuchten *et al.* (1977) and Gaber *et al.* (1995) present data for non-equilibrium mass transfer experiments performed at multiple flow rates in the same apparatus. These results were analyzed in the CTRW context by Li and Ren (2009), though the calibrations presented featured wide variation in CTRW parameters between runs at different flow rates and between, e.g., $\bar{v}$ and v_ψ. While it would be worthwhile to re-analyze this data, we obtained data from the more recent column experiments of Knorr *et al.* (2016), which had never been analyzed in the context of CTRW, and which featured a complex dual-domain geometry that appeared to represent a more difficult fitting challenge. We chose to calibrate against this data set for the MIMT demonstration.

We corroborate the simplified approach and our claims about velocity invariance of $\psi(t)$ by successfully calibrating all the breakthrough curves simultaneously with identical

parameters for both data sets. We also calibrate very different CTRW parameters than presented by Berkowitz and Scher (2009) for the same system, illustrating that it is not generally possible to interpret particular parameters in terms of system features, independent of a complete model description. Rather, in line with the temporal subordination philosophy underlying the simplified approach, the complete CTRW GME parameterization must be viewed as a whole.

2 Heterogeneous advection flow cell experiment

2.1 Experimental setup

The data set was obtained from a suite of experiments previously discussed at length by Levy and Berkowitz (2003). We will only briefly recapitulate the relevant factors in the experimental setup, as full details may be found in the original paper. Tracer experiments were performed in a flow cell with length $L = 2.13$ m, which was manually packed with "blocks", each of which consisted of one of three different sands with different hydraulic conductivities. The blocks were arranged in the flow cell in such a way that a heterogeneous but spatially stationary conductivity field with an exponential correlation structure was created. Levy and Berkowitz reported flow rates for the three experiments in this cell as 175 ml min^{-1}, 74 ml min^{-1}, and 11 ml min^{-1}. Bulk cross-sectional area of the flow cell was reported as 650 cm^2, allowing Darcy flux q to be computed. Actual system porosity, n, was not measured or estimated, so actual average fluid velocity, $\bar{v}$, is not exactly known.

2.2 Numerical approach

Our goal was to numerically re-analyze these experimental results and explain all the breakthrough curves simultaneously under tight constraints: *identical* $\psi(t)$ and α, and exactly enforcing $v_\psi = \bar{v} = q/n$, for some fixed n, and $D_\psi \equiv D = \alpha\bar{v}$.

Fitting was performed by numerical Laplace transform inversion. The analytic solution of the GME (1) in the Laplace domain for a 1D semi-infinite domain has the form (Burnell *et al.*, 2017):

$$\tilde{\hat{c}}(x,s) = \frac{1}{s}\exp\left\{\frac{x}{2D}\left[\bar{v} - \sqrt{\bar{v}^2 + \frac{4Ds}{\tilde{M}(s)}}\right]\right\} \tag{5}$$

where $\tilde{M}(s)$ is as defined in (2). Based on past success, we assumed that $\psi(t)$ had truncated power law (TPL) form. The Laplace transform of the TPL is (Dentz *et al.*, 2004):

$$\tilde{\psi}(s) = (1 + t_2 s)^{\beta} \exp(t_1 s) \frac{\Gamma(-\beta, t_1 s + t_1 t_2^{-1})}{\Gamma(-\beta, t_1 t_2^{-1})}. \tag{6}$$

Note that whilst we assume that τ is unity, we do not assume that this is equal to the t_1 parameter of the TPL, in contrast with some earlier literature. In our approach, $\psi(t)$ is understood as a temporal subordination mapping corresponding to unit time, and all its parameters may be freely specified.

For a given vector of parameters, we determined the estimate $\hat{c}(x = L, t; \alpha, \beta, t_1, t_2, \bar{v})$ by numerical inversion of the Laplace transform (5) using the Fixed Talbot algorithm (Abate and Valkó, 2004) at the locations where breakthrough concentration measurements had been made. To optimize the fitting parameters, α, β, t_1, t_2, and n, we defined an equally-weighted penalty function based on the squared distance of all measured breakthrough curve data from $\hat{c}(x = L, t_i; \alpha, \beta, t_2, \bar{v})$, where t_i represents the i-th measurement time in the corresponding breakthrough curve. We used the Nelder-Mead unconstrained optimization algorithm (Nelder and Mead, 1965), as implemented in Numpy/Scipy (Oliphant, 2007), to iteratively update the five fitting parameters to improve the model fit relative to the data. The fitting parameters were represented internally as squares of dummy variables to enforce non-negativity.

2.3 Results and discussion

The optimization algorithm found a best fit with the parameters $\alpha = 5.587 \times 10^{-2}$ m, $t_1 = 1.154$ min, $t_2 = 4.011$ min, and $\beta = 0.556$, inferring porosity $n = 0.245$. In Figure 1, the experimental data are shown, along with the best fit $\hat{c}(L, t)$. It is apparent from the figure that the fitted $\hat{c}$ yields a qualitatively good fit across the all breakthrough curves. Note that despite the TPL form, the modest t_2 (representing the onset time of exponential tempering) means that this distribution is close to exponential. This accounts for the relative similarity of the empirical breakthrough curves ADE breakthrough curves, as demonstrated by Levy and Berkowitz, and expected for advection through ten or more correlation lengths of moderately heterogeneous media (see Hansen *et al.*, 2018, and references within). When $\psi(t) = e^{-t}$, it follows from (2) that $\tilde{M}(s) = 1$, or $M(t) = \delta(t)$, and the CTRW GME reduces to the ADE.

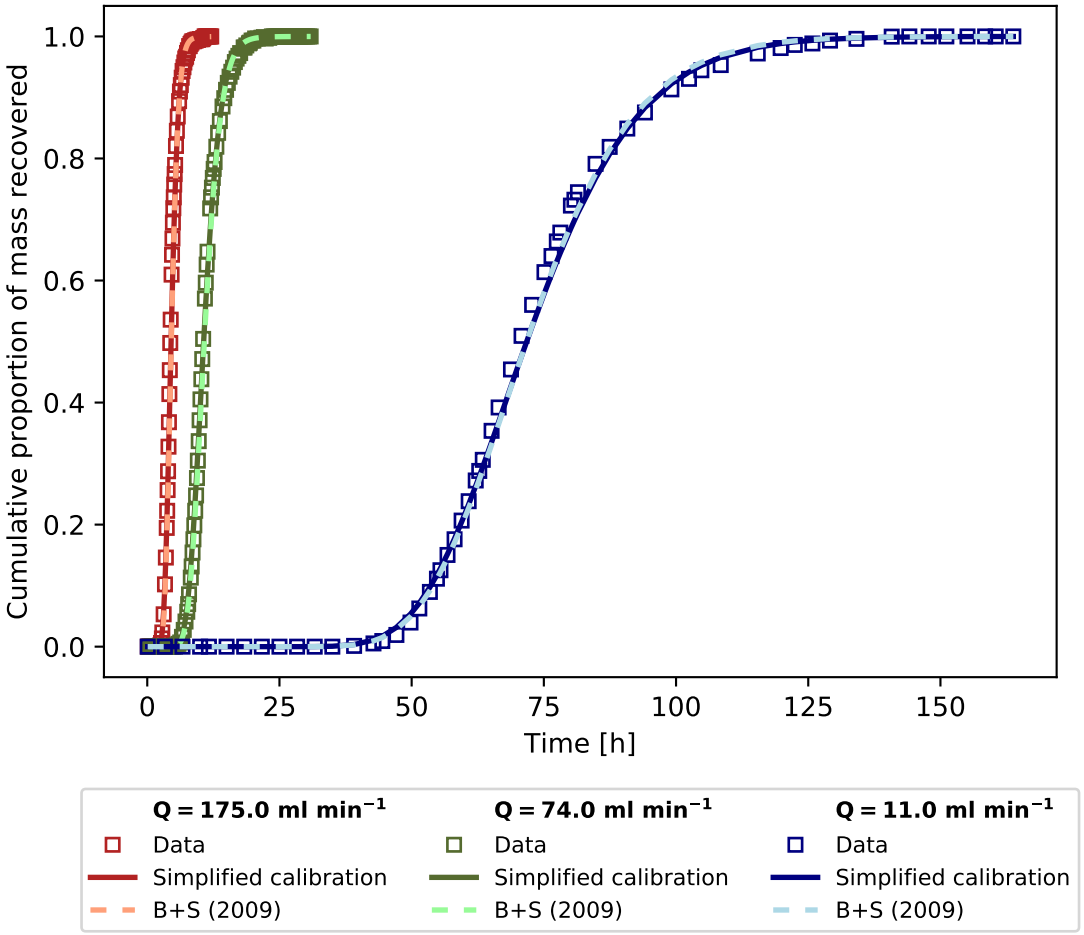

Figure 1. Simultaneous fit of three breakthrough curves collected in the flow cell described by Levy and Berkowitz (2003), at three different flow rates. Empirical breakthrough data points are indicated by hollow squares, and corresponding predicted breakthrough curves are shown as solid lines; both are colour-coded according to the corresponding flow rate. All three fitted curves shared identical $\alpha = 5.587 \times 10^{-2}$ m, fitted porosity $n = 0.245$, and TPL-distributed $\psi(t)$ (6) with parameters $t_1 = 1.154$ min, $t_2 = 4.011$ min, $\beta = 0.556$.

Berkowitz and Scher (2009) previously analyzed the same data and were able to obtain excellent fits to the breakthrough curves with separate TPL $\psi(t)$ for each flow rate that nevertheless shared two of their three parameters (t_1 was allowed to vary). We recomputed the v_ψ values reported in the original paper to three significant digits, enforcing $v_\psi \propto Q$ and $D_\psi \propto v_\psi$, each with single constants of proportionality for all three flow rates (a stipulation mentioned explicitly by the authors) by adjusting the constants of proportionality so as to generate excellent fits that closely match the published fits. We use these recomputed v_ψ values alongside the other exact, published numbers in all analyses.

The Berkowitz and Scher approach differs from ours in two major ways:

1. The earlier paper considered a "transition" to correspond to a fixed, pore-sized motion, with τ representing a characteristic time for such a motion (which naturally varies inversely with velocity). The t_1 parameter in defining the TPL $\psi(t)$ was also understood to be identified with this quantity, so $t_1 = \tau$, and varied with velocity also. By contrast, on what we dub the simplified approach, τ is understood as unit *time*, the "transition" representing notional motion occurring in unit time under macroscopic advective-dispersive conditions, and $\psi(t)$ as a mapping to the actual time taken to complete that motion with all physics operative. this temporal mapping perspective supports the velocity-invariance of $\psi(t)$, as well as the independence of all its parameters from τ (which could be set arbitrarily, but is always set to unity for convenience).
2. We take v_ψ as *identified* with an actual groundwater flow velocity, and α as a fixed, velocity independent scattering rate that is a medium property. This was explicitly not the conception of Berkowitz and Scher, who estimated a systematically different mean flow velocity based on an alternative measure of porosity. That said, actual mean flow velocity cannot be directly measured, only estimated from a given flow rate and porosity. and the v_ψ used by Berkowitz and Scher could also be interpreted as a true flow velocity by use of a plausible value of porosity.

It is enlightening to compare our fits with the strikingly different ones presented by Berkowitz and Scher; see Table 1 for a comparison of fitted parameters. Notably, the distinct TPL $\psi(t)$ functions obtained for each value of Q obtained by Berkowitz and Scher for pore-scale transitions feature a lengthy power law regime and a power law exponent

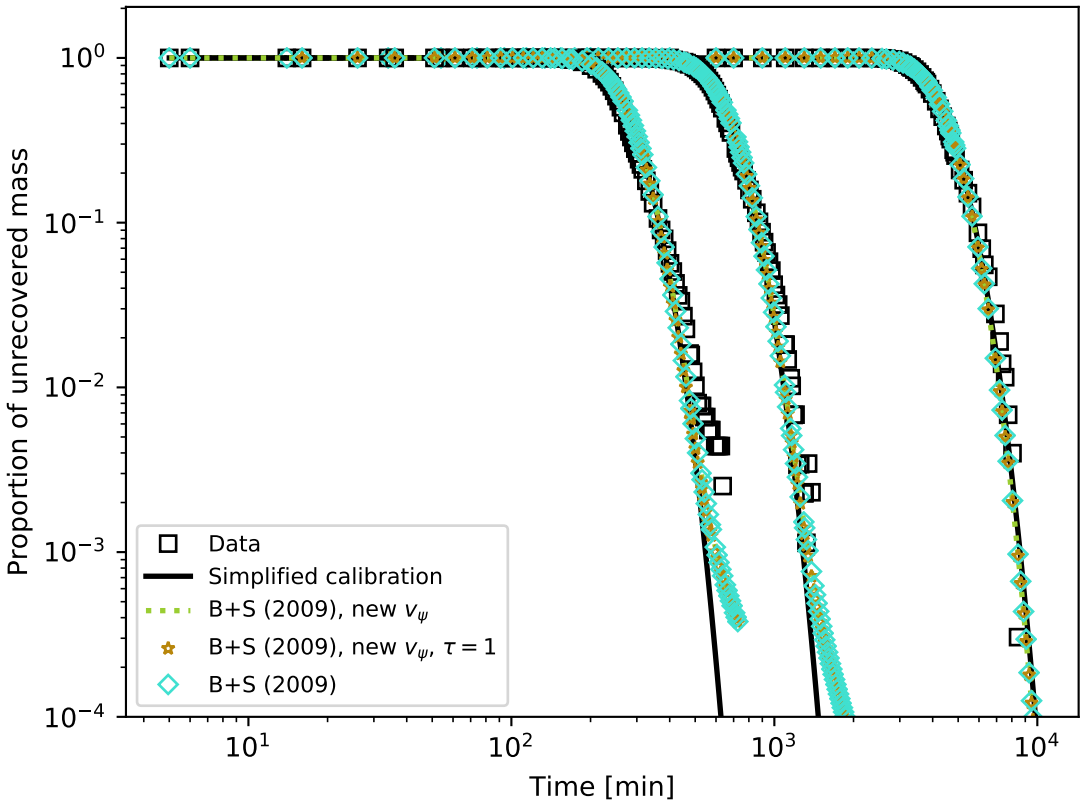

Figure 2. Comparison of ensembles of fitted breakthrough curves for all three flow rates, shown using different parameterization approaches. Curves are shown as complementary CDFs on log-log axes to highlight the tail regions. The three column groups in Table 1 are each represented, as well as a fourth approach that rescales the Berkowitz and Scher results to correspond with the velocity in the simplified calibration *and* $\tau = 1$.

$\beta = 1.6$, whereas our unified TPL fit features a much smaller value $\beta = 0.556$ and a negligible power law regime.

The breakthrough curves obtained with the velocity-dependent parameterizations of Berkowitz and Scher are visually indistinguishable from curves obtained with the simplified approach shown in Figure 1. The theoretical non-uniqueness of CTRW parameterization has previously been remarked upon (Hansen and Berkowitz, 2014). However, to our knowledge this is the first instance of near-identical calibrations being produced with completely distinct $\psi(t)$ functions. It may be initially surprising that the earlier calibrations featured

lengthy power law regions in their $\psi(t)$, whereas the new calibration does not. However, we note that because we make the identification $\tau = 1$, the implied distance covered during a transition is much larger (on the order of 10 cm at the fastest flow rate), compared with that of Berkowitz and Scher, who anticipated transitions on the order of a single pore. Consequently, much self-averaging of pore-scale transitions occur over a single notional transition on the simplified approach with $\tau = 1$. Prior to the self-averaging, CTRW parameters such as β remain meaningful as to the distribution of transition times across their implicit support scale.

In Figure 2 we compare the tail behavior of (i) our simplified approach parameterization, (ii) the parameterizations presented by Berkowitz and Scher, (iii) those same parameterizations modified to use the same v_ψ's as we did, (iv) further modified to correspond to unit τ. The latter three are identical, as the theory in Hansen (2020) predicts, and all four are essentially the same even within the tail region of the measurements. We also compare the $\psi(t)$ distributions for (i), (iii) and (iv) in Figure 3. Strikingly, we see all the distributions in (ii) map onto one-another under the transformations (iv), which follows from their being physically meaningful for their various flow rates and now sharing the same v_ψ, α, and τ. However, the $\psi(t)$ distribution predicted by (i) remains totally distinct, despite only varying in its underlying α from the transformed distributions (iv).

An important take-away from this analysis is that efforts to directly connect single parameters such as β to fundamental transport characteristics are too simple: it is crucial to consider the complete mapping $\tau \rightarrow \psi(t)$ *and also the underlying ADE model.* As we have seen, even small changes in the chosen α with otherwise identical v_ψ and τ cause drastic quantitative and qualitative changes to the $\psi(t)$ distribution needed to accurately describe observed physics.

3 Mobile-immobile column experiment

3.1 Experimental setup

Source data was obtained for a set of MIMT column experiments detailed in Knorr *et al.*; we refer readers to the original paper for more details regarding experimental setup. In brief, tracer experiments were performed in a cylindrical column whose core (mobile domain) was filled with large class beads, surrounded by an annular immobile region packed with clayey silt. The core had a radius of 1.6 cm, and the outer annulus filled the region whose radial distance from the axis was between 1.6 and 4.4 cm from the axis of the column,

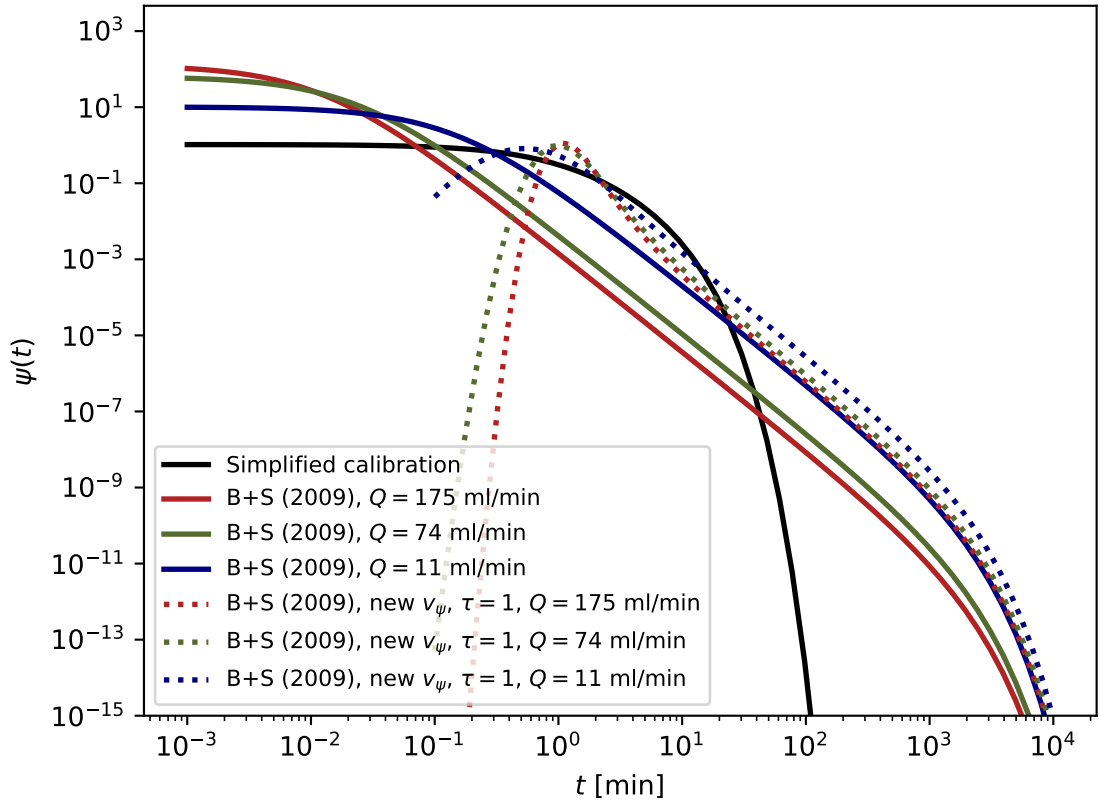

Figure 3. Comparison of transition functions, $\psi(t)$. Solid lines represent curves defined in the *Simplified calibration* (all share the same $\psi(t)$) and *B+S (2009)* column groups in Table 1. Dotted curves represent the $\psi(t)$ of B+S, interpreted according to the simplified approach; modified to share the same velocities as the simplified calibration, and also transformed in Laplace space to share the same unit value of τ.

Table 1. Comparison of fitted parameters explaining the breakthrough curves in the flow cell, as presented in this work (*Simplified calibration* meta-column), in Berkowitz and Scher, except with corrected v_ψ (*B+S (2009)* meta-column), and Berkowitz and Scher, rescaled to match the v_ψ employed in the simplified calibration (*B+S (2009), S.C.* v_ψ meta-column).

		Simplified calibration			**B+S (2009), v_ψ = S.C. $\bar{v}$**			**B+S (2009)**[1]		
Q	[ml min^{-1}]	11	74	175	11	74	175	11	74	175
$\bar{v}^2$	[m min^{-1}]	6.91e−4	4.65e−3	1.10e−2	6.91e−4	4.65e−3	1.10e−2	7.91e−4	5.31e−3	1.26e−2
n	[−]		0.245			0.245			0.214	
α	[m]		5.59e−2			5.05e−2			5.05e−2[3]	
τ	[min]		1		1.81e−2	2.87e−2	1.44e−2	1.58e−1	2.51e−2	1.26e−2
t_1	[min]		1.155		1.58e−1	2.51e−2	1.26e−2	1.58e−1	2.51e−2	1.26e−2
t_2	[min]		4.011			1000			1000	
β	[−]		0.556			1.6			1.6	

[1] Corrected velocities shown. [2] Equivalently, v_ψ. [3] From interpreting v_ψ as actual mean flow velocity, $\bar{v}$.

where it abutted a layer of silicon glue that attached it to the inner wall of the impermeable column. The column itself had internal length, L of 50 cm, with tracer-enriched fluid pumped at constant rates into the mobile domain at one end of the column and collected at the other. By measuring tracer concentrations at the column exit, breakthrough curves were obtained for a number of chemical species, each tested at volumetric flow rates of 104.4, 21, and 7.2 ml h^{-1}. The authors estimated the porosity, n, of the mobile domain as approximately $n = 0.44 \pm 1$ based on geometrical considerations and water displacement measurements.

We noted that the raw breakthrough data published by Knorr *et al.*, exhibited an implied arrival-time PDF whose integral over the real line was less then one for some flow rates, which affected the cumulative recovery time series we employed for calibration. We discuss how we rescaled the data in Appendix A. All analysis was performed using the rescaled data.

The models assumed a well-mixed mobile zone that can be treated as a 1D feature. Based on the calibrated dispersivities presented by the authors of the experimental study, we calculated that molecular diffusion was necessary to augment transverse dispersion in mixing the mobile zone of the column. Consequently, we selected the experimental

time series employing a deuterium tracer, as this species featured the largest Fickian diffusivity of those studied.

3.2 Numerical approach

Analysis was again performed by making use of the 1D analytic solution (5) for the breakthrough curve at the outlet of the column. We employed the assumption that the distribution of time between immobilization events (or until first immobilization) was exponentially distributed with parameter λ. In Appendix B we derive the Laplace transform of the sojourn time pdf for a single immobilization event as:

$$\tilde{\phi}(s) \equiv 1 - \frac{\sqrt{2\mu s}}{s+\mu}, \tag{7}$$

with μ [T^{-1}] is a free parameter proportional to the Fickian diffusion constant in the immobile zone. The CTRW transition time distribution was defined according to the relation (Margolin *et al.*, 2003; Boano *et al.*, 2007)

$$\tilde{\psi}(s) = \tilde{\psi}_0(s + \lambda - \lambda\tilde{\phi}(s)), \tag{8}$$

where $\psi_0(t)$ is the transition time distribution in the absence of MIMT. In our case, MIMT is assumed to be the only non-Fickian process, so

$$\tilde{\psi}_0(s) = \frac{1}{1+s}. \tag{9}$$

as this choice causes (2) to become unity, and (1) to thus degenerate into the ADE.

We used a similar numerical approach and algorithm to that detailed above for the flow cell experiment, with a duly modified $\tilde{\psi}(s)$. In accordance with Knorr *et al.*, we manually set $n = 0.43$ and performed Nelder-Mead automated fitting of all empirical breakthrough curves simultaneously, using the published flow rates for each experiment, to identify α, λ, and d shared by all experiments.

For comparison, we evaluated the analytical solution of Maloszewski and Zuber (1990), which was used by Knorr *et al.* to explain their experimental data. Their solution for the CDF corresponding to the CTRW model (5) may be expressed as

$$\hat{c}_{MZ}(x,t) = \frac{a}{2\pi}\sqrt{\frac{x^2}{\alpha\bar{v}}}\int_0^t\int_0^s \exp\left[-\frac{(x-u\bar{v})}{4\alpha u\bar{v}} - \frac{a^2u^2}{s-u}\right]\frac{1}{u(s-u)^3}du\ ds, \tag{10}$$

Table 2. Comparison of fitted parameters for the ensemble of curves from the MIMT column experiment. The parameters identified in this work are listed in the *Simplified calibration* meta-column, and those identified by Knorr *et al.* (2016) are lised in the corresponding meta-column. Fitted parameters from that paper have been refactored in terms of n and α for easier comparison. Note that the reported n values are explicitly identified as effective mobile porosities in Knorr *et al.*.

		Simplified calibration			**Knorr et al. (2016)**		
Q	[cm^3 h^{-1}]	7.2	21	104.4	7.2	21	104.4
v_ψ	[cm h^{-1}]	2.08	6.08	30.2	2.38	6.24	29.17
n	[−]		0.43		0.376	0.418	0.445
α	[cm]		1.30		7.6e−2	0.106	0.303
λ	[h^{-1}]		4.11			-	
μ	[h^{-1}]		1.03e3			-	
a	[h$^{-1/2}$]		-		0.105	0.100	9.48e−2

where a [T$^{-1/2}$] is a free parameter that scales with the square root of the dispersivity in the matrix. As this solution is defined in terms of a double-integral with an integrand that varies over many orders of magnitude, we employed the `mpmath` arbitrary-precision Python library (Johansson *et al.*, 2021) to perform the numerical quadrature.

3.3 Results and discussion

The optimized parameters are listed in Table 2, alongside the parameters determined by Knorr *et al.*. Predicted breakthrough curves for the ensemble of flow rates as compared with the (corrected) data is seen in Figure 4. The comparable fidelity of the two sets of curves is apparent, despite the fact that the earlier authors allowed substantial variation in what should be flow-rate-independent parameters to optimize their fits, and we did not. We observe that our model contains one more degree of freedom than the Maloszewski and Zuber model, in that it contains a distinct capture rate parameter. This is opposed to assuming the mobile domain is well-mixed, with net fluxes into the immobile zone controlled by concentration gradients in the immobile zone alone.

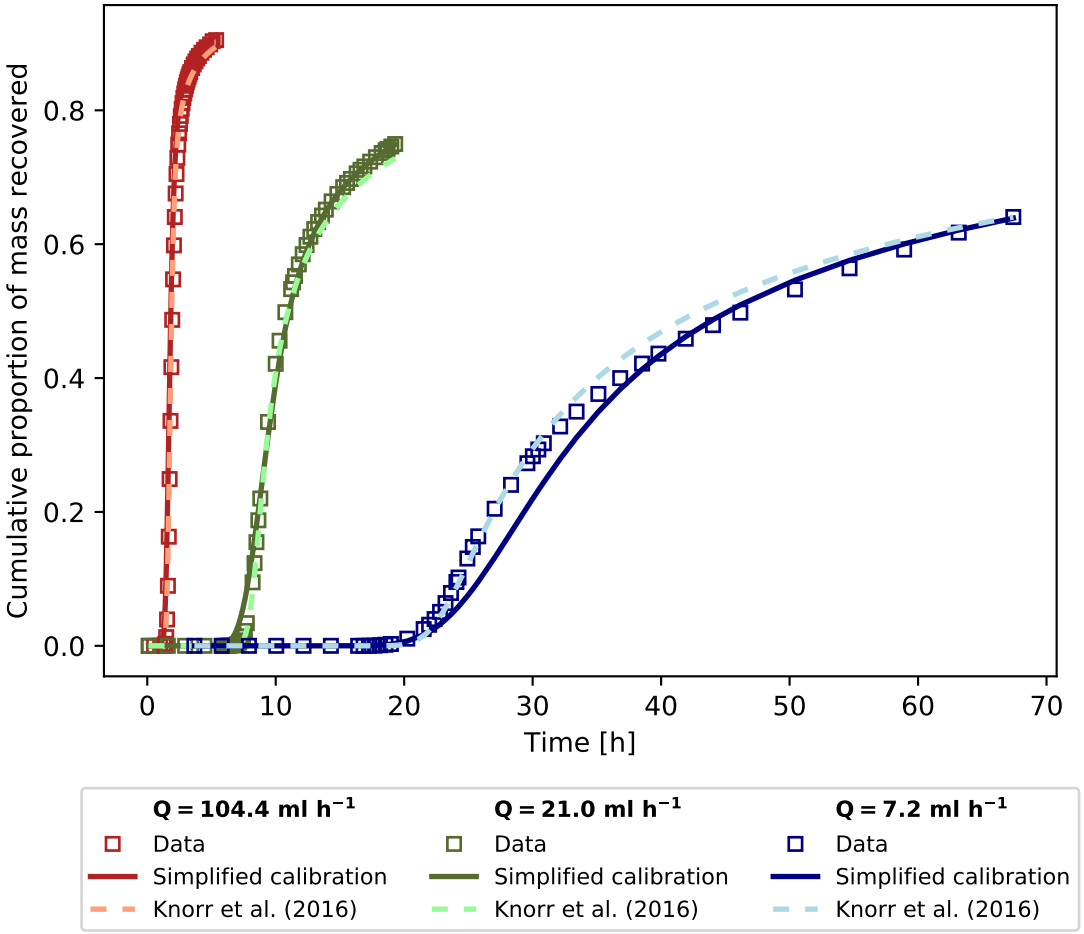

Figure 4. Simultaneous fit of three breakthrough curves collected in the column described by Knorr *et al.* (2016), at three different flow rates. Empirical breakthrough data (as adjusted per Appendix Appendix A) is indicated by empty squares, the original fits using (10) are indicated by dashed lines, and the joint calibration performed here is indicated by solid lines.

4 Summary discussion

4.1 The simplified approach is empirically supported

We re-analyzed two sets of bench-scale transport experiment data, one exhibiting HA and the other exhibiting MIMT, using the simplified approach to CTRW calibration that we previously derived. On this approach, the velocity-like and dispersion-like parameters in the CTRW GME are set equal to their Fickian counterparts, and the time constant is set to unity.

These results provide empirical support for the claims that mean groundwater velocity and a velocity-independent classical dispersivity suitable to domain scale can be employed directly in the CTRW GME, rather than the velocity-like and dispersion-like parameters v_ψ and D_ψ. It also supports the notion that $\psi(t)$ can be considered as a *temporal mapping* (subordination mapping) encoding the transition time alteration by physical processes not captured by mean advection ($\bar{v}$) and Fickian dispersion (D), namely MIMT and small-scale advective heterogeneity. The results simultaneously support the qualitative arguments underpinning the CTRW-on-a-streamline numerical approach which support the usage of a velocity-invariant $\psi(t)$ for HA and MIMT.

4.2 CTRW parameters cannot generally be interpreted in isolation

When interpreting the heterogeneous tank experiment, we parameterized a CTRW model with a TPL $\psi(t)$ featuring parameters much different from the previous calibration of Berkowitz and Scher. Most notably, both calibrations featured shared values of β and t_2 for all flow rates, but the calibrated values differ greatly between the two works. Li and Ren (2009) write "[t]he function $\psi(t)$ is the "heart" of the CTRW formation, dominating the principal characteristics of solute plume migration patterns....[t]he key factor is the interplay between β and the cutoff time t_2, which has a dramatic effect on the entire shape of a migrating solute plume." The key point is the *interplay* of parameters in the model. Stronger statements implying that individual parameters may be interpreted in isolation are also found in the literature. For example, Shahmohammadi-Kalalagh and Beyrami (2015) write "the single parameter β quantifies all of the mechanisms that control the transport behavior". In this spirit, some authors only report the value of β when performing CTRW fits using TPL-distributed $\psi(t)$, but not t_1 or t_2. (e.g., Xiong *et al.*, 2006; Shahmohammadi-Kalalagh and Beyrami, 2015; Frank *et al.*, 2020; Hu *et al.*, 2020), or report all TPL parameters

alongside v_ψ and D_ψ but do not report τ (e.g. Mettier *et al.*, 2006; Heidari and Li, 2014; Jiménez-Hornero *et al.*, 2005).

Our HA calibration above showed that the same set of experimentally-derived breakthrough curves can be parameterized with very different shared β and $t_2 - t_1$, both generating excellent, essentially indistinguishable breakthrough curve fits. This provides a cautionary counterexample to relating single CTRW parameters to underlying physics in isolation: one should report the complete transport description. This observation naturally extends to any mathematical formulation of $\psi(t)$, and to other superficially different approaches (e.g., multi-rate mass-transfer and fractional derivative models, see Berkowitz *et al.* (2006)) that are special cases of the CTRW.

The need for this *particular* parameter set is tied to the use of (4): where one is working with explicit advective transitions, sometimes termed a time-domain random walk (Cvetkovic *et al.*, 2014; Hansen and Berkowitz, 2014; Cvetkovic *et al.*, 2016; Hansen and Berkowitz, 2020b), implicit advective transitions across voxels (Bijeljic *et al.*, 2011; Edery *et al.*, 2014), or where calibration uses a first-passage distribution based on a pure power law $\psi(t)$ (Margolin and Berkowitz, 2000; Kosakowski *et al.*, 2001; Bromly and Hinz, 2004), fewer parameters may be needed for a complete model description. In all cases, however, a complete model description must be reported to ensure meaningful, repeatable results, regardless of the model formulation.

As CTRW has demonstrated predictive validity (Fiori *et al.*, 2015), it is natural to relate its parameters to underlying physics by regression and other approaches. Recent examples include Edery (2021), which explored the relationship between the difference $t_2 - t_1$ and conductivity field heterogeneity, and Frank *et al.* (2020) developed a regression relationship between β for a fracture transport and the Hurst exponent representing fracture roughness. In such efforts, we stress the need for a complete transport heterogeneity description when seeking physical interpretations; individual parameter values are not always uniquely constrained by physics. Fortunately, this additional complexity may be reduced without loss of generality on the simplified approach, as $(\alpha, \psi(t))$ represents a complete transport heterogeneity description, it is not necessary to include (v_ψ, D_ψ, τ) in an explanatory model.

Acknowledgments

We thank Prof. Brian Berkowitz for providing the original data for the HA flow cell experiment, Prof. Christine Stumpp for providing the original data for the MIMT column experiment, and both for helpful comments. All data used may also be digitized from the text and figures of Berkowitz and Scher (2009) and Knorr *et al.* (2016); no original data sets were employed in this paper. The work was supported by the Israel Science Foundation personal research grant 1872/19. SKH holds the Helen Unger Career Development Chair in Desert Hydrogeology at Ben-Gurion University.

References

Abate, J.; P. P. Valkó, 2004. Multi-precision Laplace transform inversion. *International Journal for Numerical Methods in Engineering*, **60**(5), 979. 10.1002/nme.995.

Berkowitz, B.; A. Cortis; M. Dentz; H. Scher, 2006. Modeling non-Fickian Transport in Geological Formations as a Continuous Time Random Walk. *Reviews of Geophysics*, **44**, RG2003. 10.1029/2005RG000178.

Berkowitz, B.; H. Scher, 2009. Exploring the nature of non-Fickian transport in laboratory experiments. *Advances in Water Resources*, **32**(5), 750. 10.1016/j.advwatres.2008.05.004.

Bijeljic, B.; P. Mostaghimi; M. J. Blunt, 2011. Signature of non-fickian solute transport in complex heterogeneous porous media. *Physical Review Letters*, **107**(20), 20. 10.1103/PhysRevLett.107.204502.

Boano, F.; A. I. Packman; A. Cortis; R. Revelli; L. Ridolfi, 2007. A continuous time random walk approach to the stream transport of solutes. *Water Resources Research*, **43**(10), 1. 10.1029/2007WR006062.

Bromly, M.; C. Hinz, 2004. Non-Fickian transport in homogeneous unsaturated repacked sand. *Water Resources Research*, **40**(7), 1. 10.1029/2003WR002579.

Burnell, D. K.; S. K. Hansen; J. Xu, 2017. Transient modeling of non-Fickian transport and first-order reaction using continuous time random walk. *Advances in Water Resources*, **107**, 370. 10.1016/j.advwatres.2017.06.014.

Cvetkovic, V.; A. Fiori; G. Dagan, 2014. Solute transport in aquifers of arbitrary variability: A time-domain random walk formulation. *Water Resources Research*,

50, 5759. 10.1111/j.1752-1688.1969.tb04897.x.

Cvetkovic, V.; A. Fiori; G. Dagan, 2016. Tracer travel and residence time distributions in highly heterogeneous aquifers: Coupled effect of flow variability and mass transfer. *Journal of Hydrology*, **543**, 101. 10.1016/j.jhydrol.2016.04.072.

Dentz, M.; A. Cortis; H. Scher; B. Berkowitz, 2004. Time behavior of solute transport in heterogeneous media: Transition from anomalous to normal transport. *Advances in Water Resources*, **27**, 155. 10.1016/j.advwatres.2003.11.002.

Edery, Y., 2021. The effect of varying correlation lengths on anomalous transport. *Transport in Porous Media*, **137**(2), 345. 10.1007/s11242-021-01563-9.

Edery, Y.; A. Guadagnini; H. Scher; B. Berkowitz, 2014. Origins of anomalous transport in heterogeneous media: Structural and dynamic controls. *Water Resources Research*, **50**, 1490. 10.1002/2013WR015111.

Fiori, A.; A. Zarlenga; H. Gotovac; I. Jankovic; E. Volpi; V. Cvetkovic; G. Dagan, 2015. Advective transport in heterogeneous aquifers: Are proxy models predictive? *Water Resources Research*, **51**, 9127.

Frank, S.; T. Heinze; S. Wohnlich, 2020. Comparison of surface roughness and transport processes of sawed, split and natural sandstone fractures. *Water (Switzerland)*, **12**(9). 10.3390/w12092530.

Gaber, H. M.; W. P. Inskeep; S. D. Comfort; J. M. Wraith, 1995. Nonequilibrium Transport of Atrazine through Large Intact Soil Cores. *Soil Science Society of America Journal*, **59**(1), 60. 10.2136/sssaj1995.03615995005900010009x.

Haggerty, R.; S. A. McKenna; L. C. Meigs, 2000. On the late-time behavior of tracer test breakthrough curves. *Water Resources Research*, **36**(12), 3467. 10.1029/2000WR900214.

Hansen, S. K., 2020. Simplified calibration of continuous-time random walk solute transport models. *Advances in Water Resources*, **137**, 103521. 10.1016/j.advwatres.2020.103521.

Hansen, S. K.; B. Berkowitz, 2014. Interpretation and nonuniqueness of CTRW transition distributions: Insights from an alternative solute transport formulation. *Advances in Water Resources*, **74**, 54. 10.1016/j.advwatres.2014.07.011.

Hansen, S. K.; B. Berkowitz, 2020a. Aurora: A non-Fickian (and Fickian) particle tracking package for modeling groundwater contaminant transport

with MODFLOW. *Environmental Modelling and Software*, **134**, 104871. 10.1016/j.envsoft.2020.104871.

Hansen, S. K.; B. Berkowitz, 2020b. Modeling non-Fickian solute transport due to mass transfer and physical heterogeneity on arbitrary groundwater velocity fields. *Water Resources Research*, **56**, e2019WR026868. 10.1029/2019WR026868.

Hansen, S. K.; C. P. Haslauer; O. A. Cirpka; V. V. Vesselinov, 2018. Direct Breakthrough Curve Prediction From Statistics of Heterogeneous Conductivity Fields. *Water Resources Research*, **54**(1), 271. 10.1002/2017WR020450.

Heidari, P.; L. Li, 2014. Solute transport in low-heterogeneity sandboxes: The role of correlation length and permeability variance. *Water Resources Research*, **50**, 8240. 10.1002/2013WR014654.

Hu, Y.; W. Xu; L. Zhan; Z. Ye; Y. Chen, 2020. Non-Fickian solute transport in rough-walled fractures: The effect of contact area. *Water (Switzerland)*, **12**(7). 10.3390/w12072049.

Huang, K.; N. Toride; M. T. Van Genuchten, 1995. Experimental investigation of solute transport in large, homogeneous and heterogeneous, saturated soil columns. *Transport in Porous Media*, **18**(3), 283. 10.1007/BF00616936.

Jiménez-Hornero, F. J.; J. V. Giráldez; A. Laguna; Y. Pachepsky, 2005. Continuous time random walks for analyzing the transport of a passive tracer in a single fissure. *Water Resources Research*, **41**(4), 1. 10.1029/2004WR003852.

Johansson, F.; *et al.*, 2021. *mpmath: a Python library for arbitrary-precision floating-point arithmetic (version 1.2.0)*. `http://mpmath.org/`.

Knorr, B.; P. Maloszewski; F. Krämer; C. Stumpp, 2016. Diffusive mass exchange of non-reactive substances in dual-porosity porous systems - column experiments under saturated conditions. *Hydrological Processes*, **30**(6), 914. 10.1002/hyp.10620.

Kosakowski, G.; B. Berkowitz; H. Scher, 2001. Analysis of field observations of tracer transport in a fractured till. *Journal of Contaminant Hydrology*, **47**(1), 29. 10 .1016/S0169-7722(00)00140-6.

Levy, M.; B. Berkowitz, 2003. Measurement and analysis of non-Fickian dispersion in heterogeneous porous media. *Journal of Contaminant Hydrology*, **64**(3-4), 203. 10.1016/S0169-7722(02)00204-8.

Li, N.; L. Ren, 2009. Application of continuous time random walk theory to nonequilibrium transport in soil. *Journal of Contaminant Hydrology*, **108**(3-4),

134. 10.1016/j.jconhyd.2009.07.002.

Maloszewski, P.; A. Zuber, 1990. Mathematical Modeling of Tracer Behavior in Short-Term Experiments in Fissured Rocks. *Water Resources Research*, **26**(7), 1517.

Margolin, G.; B. Berkowitz, 2000. Application of continuous time random walks to transport in porous media. *Journal of Physical Chemistry B*, **104**(16), 3942. 10 .1021/jp993721x.

Margolin, G.; M. Dentz; B. Berkowitz, 2003. Continuous time random walk and multirate mass transfer modeling of sorption. *Chemical Physics*, **295**, 71. 10.1016/j.chemphys.2003.08.007.

Mettier, R.; G. Kosakowski; O. Kolditz, 2006. Influence of small-scale heterogeneities on contaminant transport in fractured crystalline rock. *Ground Water*, **44**(5), 687. 10.1111/j.1745-6584.2006.00236.x.

Nelder, J. A.; R. Mead, 1965. A simplex method for function minimization. *The Computer Journal*, **7**, 308.

Oliphant, T. E., 2007. Python for Scientific Computing. *Computing in Science and Engineering*, **9**, 10. 10.1109/MCSE.2007.58.

Roberts, G. E.; H. Kaufman, 1966. *Table of Laplace Transforms*. W. B. Saunders Company, Philadelphia.

Shahmohammadi-Kalalagh, S.; H. Beyrami, 2015. Modeling Bromide Transport in Undisturbed Soil Columns with the Continuous Time Random Walk. *Geotechnical and Geological Engineering*, **33**(6), 1511. 10.1007/s10706-015-9917-1.

Silliman, S. E.; E. S. Simpson, 1987. Laboratory evidence of the scale effect in dispersion of solutes in porous media. *Water Resources Research*, **23**(8), 1667.

van Genuchten, M. T.; P. J. Wierenga; G. A. O'Connor, 1977. Mass Transfer Studies in Sorbing Porous Media: III. Experimental Evaluation with 2,4,5- T. *Soil Science Society of America Journal*, **41**(2), 278. 10.2136/sssaj1977 .03615995004100020023x.

Xiong, Y.; G. Huang; Q. Huang, 2006. Modeling solute transport in one-dimensional homogeneous and heterogeneous soil columns with continuous time random walk. *Journal of Contaminant Hydrology*, **86**(3-4), 163. 10.1016/j.jconhyd.2006.03.001.

Appendix A Correction of data in Knorr et al. (2016)

In Knorr *et al.* (2016), the authors present exit-time CDFs intended to correspond to (10), which have been numerically integrated from impulse response breakthrough curves that were measured. As reported, the impulse response curves should correspond to the function

$$\zeta(x,t) = \frac{a}{2\pi Q}\sqrt{\frac{x^2}{\alpha\bar{v}}}\int_0^s \exp\left[-\frac{(x-u\bar{v})}{4\alpha u\bar{v}} - \frac{a^2u^2}{t-u}\right]\frac{1}{u(t-u)^3}du, \tag{A1}$$

and $Q\zeta(L,t)$ should be the arrival time PDF at the exit of the column. As the integral of any probability distribution is 1, multiplying the reported impulse response data by Q and numerically integrating should yield 1, also. However, for the two lowest flow rates, this was not the case. Multiplying $Q\zeta(L,t)$ (as populated with the exact parameters reported by Knorr *et al.*) by the respective scaling factors 1, .82, and .625 for the flow rates 104.4, 21, and 7.2 ml h^{-1}, near-exactly reproduces the fitted impulse response curves shown in the paper. (See Figure A1 for illustration.) We verified that the CDFs reported were also generated by integration of the data shown (as pre-multiplied by Q), so the reported CDF data are off by the same factor and some total recovery rates were larger than previously shown.

Thus, the raw deuterium CDFs presented need to be multiplied respectively by 1, 1/.82, and 1/.625 to yield actual fraction recovered. We used these altered CDFs for the fitting work. We note that that the parameters in Knorr *et al.* actually also match the correctly re-scaled data when inserted into (10).

Appendix B Derivation of sojourn time PDF

We are interested in the time taken for a particle entering the immobile zone to complete its sojourn and exit. We map radial diffusion in the matrix onto a simple 1D lattice continuous-time random walk, and ask how long it takes for a particle introduced at node 0 at time 0 to return to node zero. We imagine that the lattice nodes are non-uniformly spaced (growing denser with greater radial distance), so that the transition statistics are the same for every node. Employing the observation of Knorr *et al.* that solute never reached the outside of the column, making the immobile domain an essentially infinite 1D diffusive sink, we work on a simple, infinite 1D lattice.

We define $R(x,t)$ as the ensemble average arrival rate of random walkers at node x time t, and $\psi(t)$ as the (location-independent) waiting time PDF for the time between

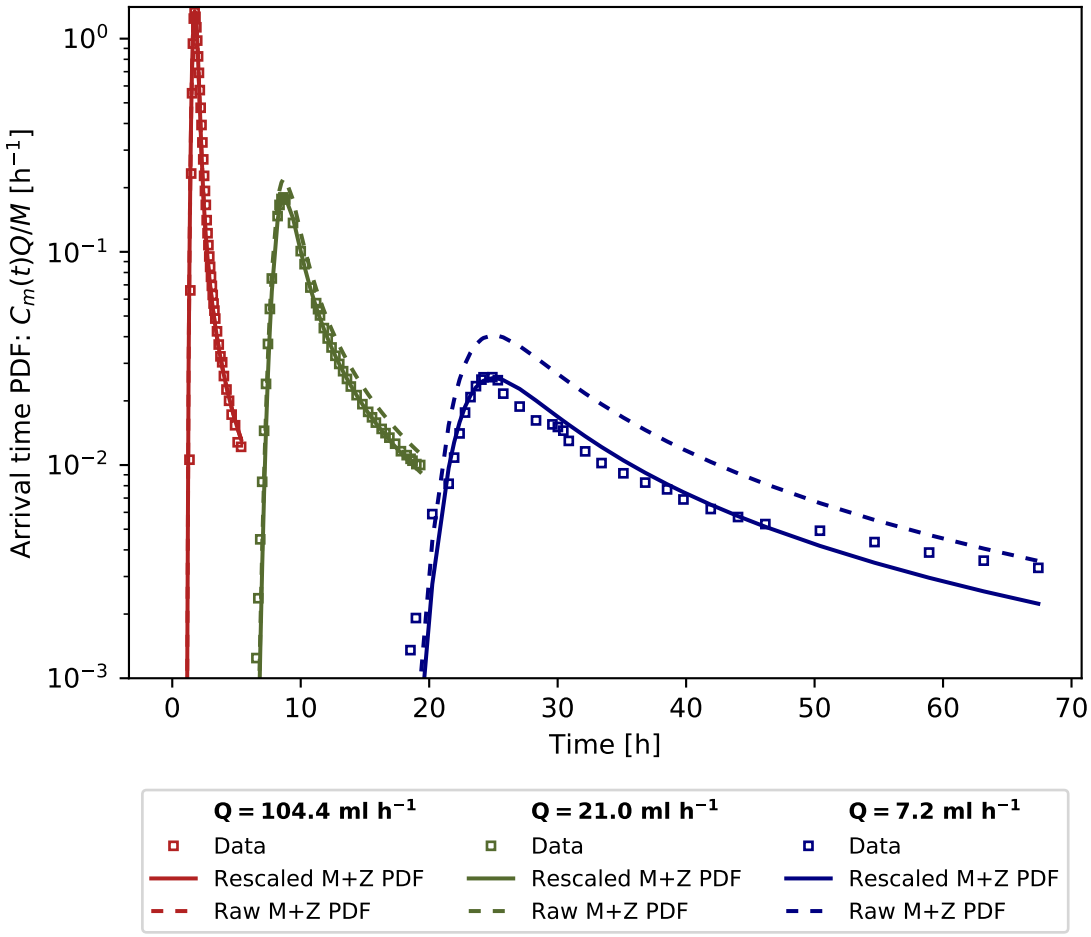

Figure A1. Data points presented in Knorr *et al.* (2016), along with raw evaluation of (A1) with parameters presented by Knorr *et al.*, and rescaled (A1) to best match the data points (and the curves shown by Knorr *et al.*).

two subsequent arrivals. Then, the ensemble average number of walkers, $P(x,t)$, at any given node, x, at time t may be expressed

$$P(x,t) = \int_0^t R(x,\tau)\Psi(t-\tau)d\tau, \tag{B1}$$

where

$$\Psi(t) \equiv 1 - \int_0^t \psi(\tau)d\tau. \tag{B2}$$

We consider a 1D system in which particles are introduced at $x = 0$ at $t = 0$ (this is the counterpart to immobilization under MIMT), and are interested in the *next* time the walker arrives at $x = 0$ (which we take to represent re-mobilization). We use the notation R_i to represent the arrival rate of only those particles that are arriving for the i-th time. Then we may write

$$R_1(0,t) = \delta(t), \tag{B3}$$

and define the sojourn time PDF

$$\phi(t) \equiv R_2(0,t). \tag{B4}$$

From recursive arguments, we may also conclude that:

$$R(x,t) = R_1(x,t) + \int_0^t R_2(x,\tau)R(0,t-\tau)d\tau, \tag{B5}$$

and thus specifically that

$$R(0,t) = \delta(t) + \int_0^t \phi(t)R(0,t-\tau)d\tau. \tag{B6}$$

Taking the Laplace transform and rearranging, yields

$$\tilde{R}(0,s) = \frac{1}{1-\tilde{\phi}(s)}. \tag{B7}$$

Transforming (B1) and applying it to the above equation yields

$$\tilde{\phi}(s) = 1 - \frac{\tilde{\Psi}(s)}{\tilde{P}(0,s)}. \tag{B8}$$

In order to determine the transform for ϕ, we must determine the transforms on the RHS of (B8), which we may do from the well-known property that the variance σ_x^2 of a plume undergoing Fickian diffusion increases according to

$$\frac{d\sigma_x^2}{dt} = 2D, \tag{B9}$$

where D here is not to be confused with D_ψ. Fickian diffusion from a point source at $x = 0$ is known to be described by a Gaussian distribution. At $x = 0$ the exponential portion of the distribution becomes unity and, mapping to a discrete-site approach with spacing Δ_x, it follows that

$$P(0,t) = \frac{\Delta_x}{\sqrt{4\pi D t}} = \frac{1}{2\pi\mu t}, \tag{B10}$$

where we define $\mu \equiv 2D/\Delta_x^2$. Taking the Laplace transform (Roberts and Kaufman, 1966), it follows that

$$\tilde{P}(0,s) = \frac{1}{\sqrt{2\mu s}}. \tag{B11}$$

We can similarly argue from (B9) that $\mu\ dt$ is the constant probability of completing a diffusive transition to a neighboring site in a short increment of time dt, implying that $\psi(t) = \mu e^{-\mu t}$, and

$$\tilde{\Psi}(s) = \frac{1}{s+\mu}. \tag{B12}$$

Inserting (B11) and (B12) into (B8) yields our final result (7), repeated here for clarity of presentation:

$$\tilde{\phi}(s) = 1 - \frac{\sqrt{2\mu s}}{s+\mu}.$$

By numerical inversion, we can see that the distribution defined by $\phi(t)$ is closely approximated by Pareto($\mu^{-1}, \frac{1}{2}$), where the first argument is the scale parameter, and $\frac{1}{2}$ is the shape parameter (power law exponent). This agrees with the with Haggerty *et al.* (2000) who reported the return time for diffusion in an infinite slab as power-law distributed (with exponent $\beta = 0.5$). Examples are shown in Figure B1.

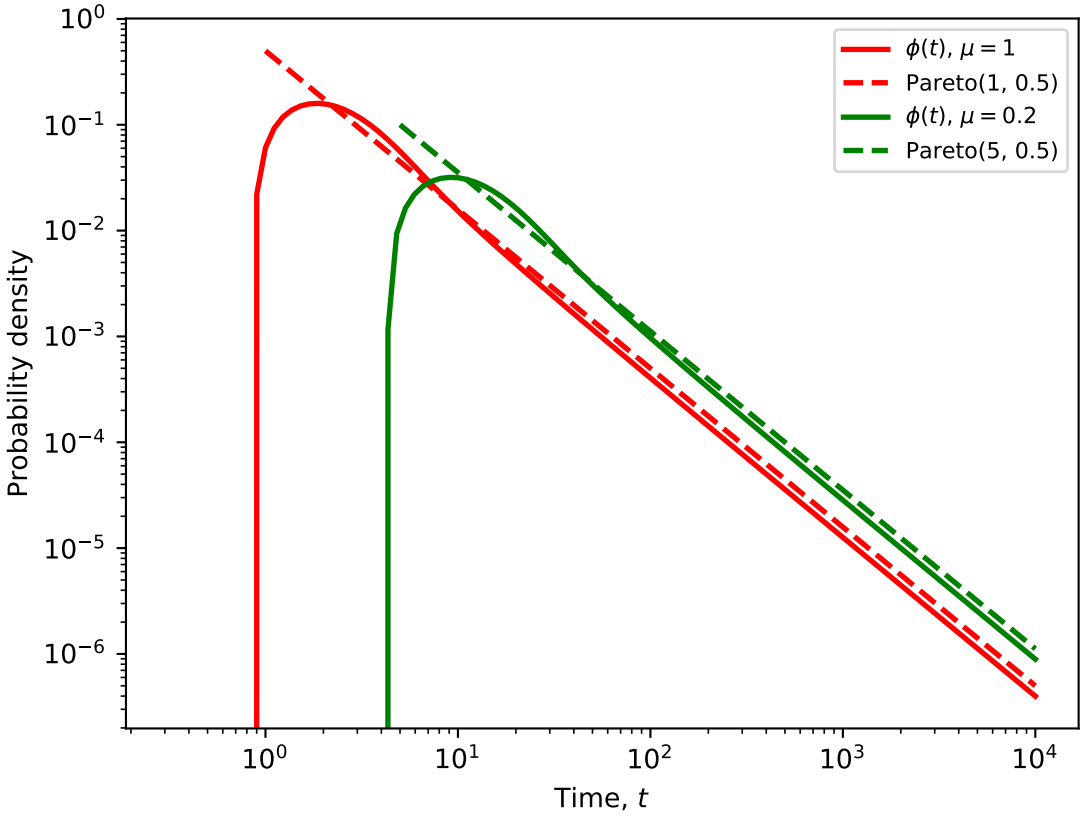

Figure B1. Graphs of $\phi(t)$ obtained from numerical inversion of (7) and corresponding Pareto approximations for two values of μ.